

Using Pressure- and Temperature-Sensitive Paint for Global Surface Pressure and Temperature Measurements on the Aft-Body of a Capsule Reentry Vehicle

A. Neal Watkins,¹ Gregory M. Buck,² Bradley D. Leighty,³ and William E. Lipford,⁴
NASA Langley Research Center, Hampton, VA 23681, USA

and

Donald M. Oglesby⁵
ATK, Hampton, VA 23681, USA

Pressure Sensitive Paint (PSP) and Temperature Sensitive Paint (TSP) were used to visualize and quantify the surface interactions of reaction control system (RCS) jets on the aft body of capsule reentry vehicle shapes. The first model tested was an Apollo-like configuration and was used to focus primarily on the effects of the forward facing roll and yaw jets. The second model tested was an early Orion Crew Module configuration blowing only out of its forward-most yaw jet, which was expected to have the most intense aerodynamic heating augmentation on the model surface. This paper will present the results from the experiments, which show that with proper system design, both PSP and TSP are effective tools for studying these types of interaction in hypersonic testing environments.

Nomenclature

PSP	=	Pressure Sensitive Paint
TSP	=	Temperature Sensitive Paint
RCS	=	reaction control system
I	=	intensity of light emitted by PSP or TSP at some pressure or temperature
I_{REF}	=	intensity at light emitted by PSP or TSP some reference pressure or temperature
P	=	surface pressure
P_{REF}	=	reference pressure
T	=	absolute surface temperature
T_{REF}	=	reference temperature
$A(T), B(T)$	=	temperature dependent calibration coefficients for PSP
$K_{SV}(T)$	=	temperature dependant Stern-Volmer coefficient
UV	=	ultraviolet
LED	=	light emitting diode
$Pt(TfPP)$	=	platinum meso-tetra(pentafluorophenyl) porphine
$Rubpy$	=	ruthenium tris-bypyridine
FEM	=	fluoroethylmethacrylate-isobutylmethacrylate co-polymer
G_1, G_2	=	time gates used for lifetime-based data acquisition
a_{xy}	=	constants for expanded PSP calibration model
b_x	=	constants for TSP calibration model
C_h	=	convective heat transfer coefficient based on enthalpy
C_{hFR}	=	convective heat transfer coefficient calculated using the method of Fay and Riddell

¹ Electronics Engineer/Chemist, Advanced Sensing and Optical Measurement Branch, Mail Stop 493

² Aerospace Technologist, Aerothermodynamics Branch, Mail Stop 408A, AIAA Member

³ Engineering Technician, Advanced Sensing and Optical Measurement Branch, Mail Stop 493

⁴ Engineering Technician, Advanced Sensing and Optical Measurement Branch, Mail Stop 493

⁵ Research Chemist, NASA Langley Research Center, Mail Stop 493

β	=	substrate thermal product
β_{REF}	=	approximation of the thermal product
θ	=	normalized thermal parameter
$Z\{\theta(T_s)\}$	=	function based on the normalized thermal parameter
h_{SO}	=	low temperature enthalpy
T_{SO}	=	surface temperature used to calculate h_{SO}
t	=	time image was taken
t_{REF}	=	reference time for image acquisition
P_j	=	jet pressure at the RCS nozzle
$P_{T,2}$	=	pressure at stagnation point on the model
$P_j/P_{T,2}$	=	jet pressure ratio

I. Introduction

The accurate determination of spatially continuous pressure and temperature distributions on aerodynamic surfaces is critical for the understanding of complex flow mechanisms and for comparison with computational fluid dynamics (CFD) predictions. This is especially true in hypersonic flight conditions for vehicle concepts such as reentry capsules, where complex flow phenomena such as flow transition, shock layer interactions, impinging jets, etc., often occur. Conventional pressure measurements are based on pressure taps and electronically scanned pressure transducers. While these approaches provide accurate pressure information, pressure taps are limited to providing data at discrete points, thus making it difficult to measure surface pressures between these locations. Moreover, the integration of a sufficient number of pressure taps on a surface can be time and labor intensive and expensive. Likewise, surface temperatures can be measured using discrete thermocouples or globally using infrared thermography. For discrete temperature measurements, similar limitations exist as for pressure taps while infrared thermography typically requires expensive equipment and windows that may not be readily available. Applying pressure sensitive paint (PSP) and temperature sensitive paint (TSP) provide alternatives for acquiring these critical global surface properties. The purpose of this work is to assess the feasibility of using PSP and TSP to visualize and quantify the surface interaction of reaction control system (RCS) jets impinging on the aft body surface of capsule reentry vehicle concepts. The highly complex topic of jet plume impingement on capsule reentry vehicles is beyond the scope of this paper, but is more adequately described by Buck *et al.*¹ and references therein.

A. Pressure Sensitive Paint

PSP is an optical diagnostic capable of recovering global surface pressure distributions on test models.²⁻⁶ The technique exploits oxygen-sensitive luminescent molecules that are dispersed in polymer binders, or paints. In wind tunnel applications, the PSP is applied to the model by conventional paint spraying techniques. Light sources such as arrays of ultraviolet (UV) light emitting diodes (LEDs) are mounted external to the test section to illuminate the painted model and effect luminescence emission from the entrapped oxygen-sensitive molecules. For the majority of pressure paints, PSP emission occurs in the orange to red region of the visible spectrum (~590 - ~650 nm). The emission intensity is inversely proportional to the amount of oxygen present at the PSP surface, such that paint regions producing more emission indicate lower concentrations of oxygen relative to paint regions producing less emission. If the test gas used in the tunnel is air, the paint emission intensity can be correlated to the total pressure at the model surface since oxygen is a fixed component in air. CCD cameras with spectral band-pass filters to discriminate between the excitation (UV) and emission (orange to red) signals capture the intensity image of the PSP-coated model surface, providing a means to recover global surface pressure distributions on test articles of interest. All PSP measurement systems employ a ratio of image pairs to compensate for intensity non-uniformity caused by effects other than pressure. The most significant of these are the consistency of the paint application and illumination heterogeneity.

If the test surface under study is immersed in an atmosphere containing O₂ (e.g. air), the recovered luminescence intensity can be described by the Stern-Volmer relationship⁷

$$I_0 / I = 1 + K_{SV}(T)P_{O_2} \quad (1)$$

where I_0 is the luminescence intensity in the absence of O₂ (i.e. vacuum), I is the luminescence intensity at some partial pressure of oxygen P_{O_2} , and $K_{SV}(T)$ is the temperature dependent Stern-Volmer constant. Since it is a practical impossibility to measure I_0 in a wind tunnel application, a modified form of the Stern-Volmer equation is typically used. This form replaces the vacuum calibration (I_0) with a reference standard⁴

$$I_{REF} / I = A(T) + B(T) \times (P/P_{REF}) \quad (2)$$

where I_{REF} is the recovered luminescence intensity at a reference pressure, P_{REF} . $A(T)$ and $B(T)$ are temperature dependent constants for a given PSP formulation and are usually determined before hand using laboratory calibration procedures.

There are two methods for acquiring PSP data. The most common method used for data acquisition is an “intensity-based” technique. During intensity-based PSP experiments, I_{REF} is typically acquired while the wind tunnel is off or at very low speed and P_{REF} is the static pressure when no wind is applied. Thus I_{REF} is referred to as the “wind-off” intensity. I is the recovered luminescence intensity at some pressure P . Since this data is collected at a specific condition in the wind tunnel, I is also referred to as the “wind-on” intensity.

A second method of PSP data acquisition is known as “lifetime-based” PSP.⁸⁻¹² In the lifetime-based technique, excitation of the PSP is accomplished using a modulated light source (e.g. laser, flash lamp, or pulsed LED arrays). A fast framing camera (intensified CCD or interline transfer CCD) is used to collect the excited state luminescence decay. Typically the decay is approximated by acquiring two or more images at different delay times during and/or after the pulsed excitation and integrating photons for fixed periods of time (i.e. gate widths) that have been predetermined to maximize the pressure sensitivity, as demonstrated in Fig. 1. The first image (Gate 1) usually consists of a short gate width and is collected either during the excitation pulse or shortly after it ends. This can be thought of as the reference image because the excited-state decay has the least pressure sensitivity. The second image (Gate 2) typically has an equal or longer gate width than Gate 1, but is taken at a later time after the excitation pulse, ensuring maximum pressure (and temperature) sensitivity.

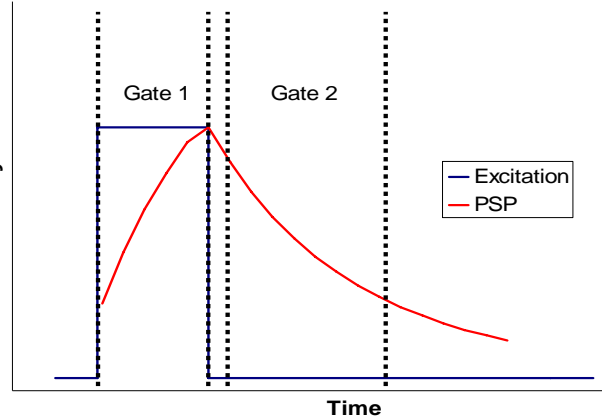


Figure 1. Schematic representation of lifetime-based data acquisition showing excitation (blue) and measured emission (red). The gate regions represent example Gate 1 (during excitation) and Gate 2 (after excitation).

The lifetime method was chosen for the PSP portion of the test because all data is taken at the run conditions. The facility that was used for the investigations uses a model injection system in which the model is held in a separate chamber until ready for use. Once the air-flow in the test section is established and consistent, the model is then injected into the flow. To use the standard intensity-based data acquisition technique, a reference image would need to be acquired at wind-off conditions; however, due to the tunnel operation procedure, accurate determination of the reference pressure was difficult as the overall tunnel pressure changes rapidly once flow is initiated. Another consideration for the lifetime-based technique is that the temperature changes between the reference and run images (Gate 1 and Gate 2) are fairly minimal because both images are taken in the flow.

B. Temperature Sensitive Paint

Global surface heat transfer measurements have been widely reported at NASA Langley Research Center (LaRC) using such techniques as thermographic phosphor coatings¹³⁻¹⁵ and infrared thermography.¹⁶ However, these techniques suffer from some limitations. Thermographic phosphor coatings generally require models to be made from silica ceramic materials, require UV illumination (below 375 nm), and are more suited for higher temperature ranges exhibited on a heat shield than on an aft body. Infrared thermography suffers from limitations mentioned above, specifically expensive specialized equipment such as cameras and window materials. These techniques have been used in a variety of heat transfer measurements and transition detection experiments at speed regimes from subsonic to hypersonic and at various testing temperature ranges (from cryogenic to room temperature and above).^{5,6,13-15,17-19}

TSP is analogous to PSP except that the luminescent molecules are chosen for maximum temperature sensitivity (as opposed to minimal for PSP) and are dispersed in an oxygen *impermeable* binder to limit quenching by oxygen. Thus all quenching occurs through non-radiative temperature effects. In these regards, TSP and thermographic phosphor coatings are similar techniques and use many of the same data acquisition and analysis procedures. However, thermographic phosphors have generally been designed to work at higher temperatures, thus preclude the

use of larger molecules which accept near UV to visible excitation or polymer binders for application. Typical thermographic phosphor materials are insoluble and thus need to be suspended in an applicable ceramic binder. This typically results in rougher coatings that also exhibit aggregation of phosphor molecules (resulting in “graininess” of the images at high spatial resolutions). For TSP applications, judicious selection of the luminophore molecule can allow excitation to be accomplished using near-UV to blue light, as well as the formation of smooth coatings as the luminophore can be dissolved to form a more traditional paint-like coating. Data acquisition techniques for TSP are the same as for PSP. For this work it was necessary to acquire a large amount of data in a short time frame, so a standard intensity-based data acquisition technique was chosen, in which a “wind-off” reference image is used with a number of “wind-on” images to calculate surface temperatures.

II. Experimental

A. Paint Formulations

The PSP formulation used for this study was based on a formulation developed at NASA LaRC and described previously.²⁰ The oxygen-permeable layer is made from a co-polymer of trifluoroethylmethacrylate and isobutylmethacrylate (abbreviated FEM), in which platinum meso-tetra(pentafluorophenyl)porphine [Pt(TfPP)] is dissolved. Before application to the model, the surface was first cleaned and degreased using acetone. After drying, a white acrylic primer was applied to the surface to act as a basecoat to enhance adhesion of the FEM topcoat as well as to enhance scattering of the luminescence intensity back to the camera.

The TSP formulation used was also based on a formulation developed at NASA LaRC. In this case, the oxygen impermeable layer is a commercially available clear urethane sealant in which the luminophore ruthenium tris-bipyridine (Rubpy) is dissolved. This was applied over the same basecoat as the PSP.

B. Paint Calibration

All paint calibrations were performed separate from the wind tunnel in a laboratory calibration chamber. A PSP or TSP formulation was applied to 3-inch diameter aluminum coupons at the same time that all model pieces were being painted. These coupons were then placed in the calibration chamber and the luminescence intensity was measured at varying temperatures and pressures (for PSP) or varying temperatures (for TSP).

The current calibration chamber can not reach the extremely low pressures needed to adequately calibrate the PSP formulation for hypersonic applications (typical test section pressures are on the order of 0.07 kPa or less). To account for this, an oxygen standard was used instead of regular air for calibration. This is a viable technique because the PSP is actually an oxygen sensor and is not easily affected by pressures. To simulate the expected pressure range, a mixture of 2000 ppm oxygen in nitrogen was used for calibration, leading to an effective calibration pressure range of 0.0007 kPa to 1 kPa (assuming air is 21% oxygen, or 210,000 ppm, this effectively decreases the measured pressure by 100). The paint formulation was calibrated over these pressure ranges at temperatures ranging from 294 K to 338 K. The lifetime technique was used to calibrate the paint, with Gate 1 occurring from 0-30 μ s (the width of the excitation pulse) and Gate 2 occurring from 35-85 μ s (5 μ s after the end of the excitation pulse), similar to Fig. 1. A calibration model for the coating was derived by solving Eq. (2) for pressure in terms of the temperature and gate intensities. The calibration data showed a multi-dimensional dependence on both pressure and temperature, which can be attributed to the complex nature of oxygen diffusion into the polymer binder.⁴⁻⁶ A linear least squares algorithm was used to fit the data to a modified and expanded version of Eq. (2) above assuming a second order relationship in both temperature and pressure

$$P = (a_{11} + a_{12}T + a_{13}T^2) + (a_{21} + a_{22}T + a_{23}T^2)(G_1/G_2) + (a_{31} + a_{32}T + a_{33}T^2)(G_1/G_2)^2 \quad (3)$$

where P is the pressure, T is the absolute temperature, G_1 and G_2 are the intensities in the respective gates (analogous to I_{REF} [G_1] and I [G_2]), and a_{xy} are the calibration coefficients.

For TSP calibrations, the chamber was set to a constant pressure and the temperature increased from 273 K to 353 K. In this case, the TSP was calibrated using the intensity-based method with the LED arrays constantly illuminating the coupon. Several different pressures were examined and the paint showed essentially no sensitivity to oxygen (unable to be measured). For this range of temperatures, the data most closely fit an inverse third order model

$$T/T_{REF} = b_1 + b_2/(I_{REF}/I) + b_3/(I_{REF}/I)^2 + b_4/(I_{REF}/I)^3 \quad (4)$$

where T is the temperature, T_{REF} is the reference (“wind-off”) temperature, I and I_{REF} are the respective image intensities, and b_x are the calibration coefficients.

C. Experimental Setup

All model testing was performed in the NASA LaRC 31-inch Mach 10 wind tunnel facility, which has been described in detail previously.²¹ The 31-Inch Mach 10 facility consists of high-pressure air storage rated to a maximum pressure of 30 MPa, a 12.5-MW electrical bundle heater that heats the air to approximately 1000 K, a settling chamber, three-dimensional contoured nozzle, test section, adjustable second minimum, after-cooler, vacuum spheres, and vacuum pumps. A 5- μ m in-line filter, before the nozzle, removes particles from the air flow that can damage the ceramic phosphor models. The nozzle itself has a 2.7-cm square beryllium copper throat, and its exit height is 0.7874 m. The test section has a 0.75 m x 0.45 m tempered-glass window for optical experimental techniques. Wind tunnel models are protected from the flow as the tunnel comes to its operating condition by a door in the side wall of the test section. After the operating condition is reached, the model is injected to the tunnel centerline in approximately 0.55 s from the back side of the test section using a hydraulic injection system. Freestream Reynolds numbers obtained in this tunnel vary from $1.5 \times 10^6/\text{m}$ to $6.5 \times 10^6/\text{m}$.

A detailed description of the models used for this test is described elsewhere.¹ The models were constructed with a steel fore-body heat shield and plastic/ceramic nanocomposite aft bodies. Two distinct aft body shapes were studied. The first shape mimicked an Apollo-era design that had no protrusions while the second shape was based on an early NASA Orion design (under the Constellation program). In addition to the aft body shapes, several different RCS jet configuration pieces were also constructed to provide flexibility in experimental design. A collection of the pieces is shown in Fig. 2. Because the nanocomposite material used for the aft bodies is an insulating material, the model for PSP was coated with an additional thin layer of copper ($\sim 635 \mu\text{m}$ thick) to dissipate heat and provide a surface with near uniform temperature. In addition, three pressure taps were available to calibrate and correlate PSP results. The models were 127 mm in diameter with an angle of attack set at 24° . Each RCS jet had a $685 \mu\text{m}$ diameter throat and an exit area to throat ratio of 22.5. The RCS jet chamber pressures were set at either 1725 or 3450 kPa.

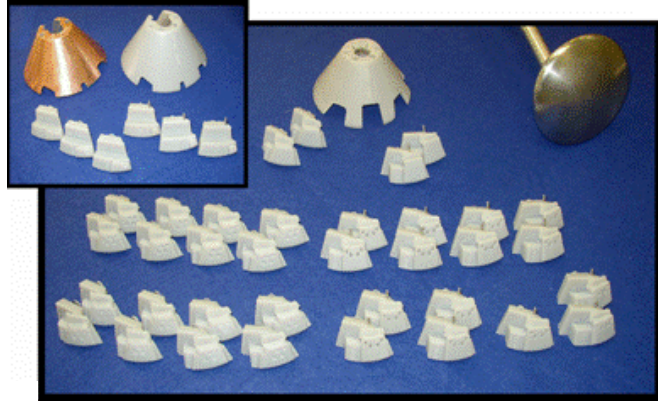


Figure 2. Aft body pieces for the Apollo-era (inset) and Orion-derived model shapes including various RCS jet configurations.

The lifetime technique was used to collect all PSP data to minimize the slight inconsistencies in sting positioning as well as the significant differences in reference temperature and pressure. Illumination was provided using four light emitting diode (LED) – based arrays. The LEDs that make up the arrays have a center wavelength of 400 nm, and the arrays are capable of high pulse rate operation. The arrays were pulsed for 30 μs at a rate of 1667 Hz to acquire all data. Images were acquired using an interline transfer camera that was modified to allow “on chip” accumulation of multiple images. The camera has an array size of 1392- x 1040- pixels and 12-bit digitization. The camera is thermoelectrically cooled to minimize shot noise. To further maximize collection efficiency, the camera was binned by 2 both horizontally and vertically (resulting image sizes are 696- x 520- pixels). The gate widths and delays are described in the calibration section above. To minimize time on centerline, only one image was acquired (using 750 LED pulses) at each gate. This resulted in a data acquisition time (both gates) to ~ 3 s, resulting in little heating as measured by embedded thermocouples.

TSP data were acquired using a standard intensity-based method. In this mode, the LED arrays were run in a continuous fashion and images were acquired using a non-interline transfer camera. This camera has an array size of 1600- x 1200- pixels and 14-bit digitization and is thermoelectrically cooled. The camera was also binned to increase collection efficiency (image sizes are 800- x 600- pixels). The reference image was acquired by injecting

the model into the test section before tunnel operation. The model was then retracted into the model box, and the tunnel started. Once tunnel conditions stabilized, the model was re-injected and data collection began. TSP images were acquired every 400 ms throughout the run, lasting 10 seconds while the model was in the tunnel on centerline.

D. Data Analysis

Analysis of the PSP images involved ratioing Gate 1 to Gate 2 and applying the calibration determined in the external calibration chamber. However, this typically resulted in a bias in the recovered pressures when compared with the taps on the model. This bias was due to small systematic errors, such as slight differences in paint application between the calibration coupon and the actual model, as well as gradients in the measured temperatures on the model. To account for this, the pressure taps were used to calculate a scaling factor that was then applied to the data. This only served to change the offset of the recovered pressures values from the PSP. It did not change the calibrated PSP pressure sensitivity. Using this technique, the PSP data typically agreed with the pressure taps to within 10%.

Analysis of the TSP images involved an additional step. As the reference image was acquired before the operation of the tunnel, a slight misalignment was seen between the wind-off and wind-on images. Dark fiducial marks were placed on the painted surface to act as targets to aid in registration of the images. Once the position of each mark was determined in each image, a second order polynomial was used to correlate the images and allow for further processing. Once correlated, the reference image was ratioed with the run image and the TSP calibration was applied. The temperature data were then used to calculate the convective heat transfer coefficient using the following relation (derived from the step solution to a one dimensional semi-infinite slab heat transfer model²²)

$$(C_h/C_{h_{FR}})(\beta_{REF}/\beta) = Z\{\theta(T_s)\}(\beta_{REF}/C_{h_{FR}})(T_{SO}/h_{SO})(t-t_{REF})^{-1/2} \quad (5)$$

where C_h is the convective heat transfer coefficient based on enthalpy, C_{hFR} is the convective heat transfer coefficient calculated using the method of Fay and Riddell,²³ β is the substrate thermal product, β_{REF} is an approximation for the thermal product, $Z\{\theta(T_s)\}$ is a function based on the normalized thermal parameter θ , T_{SO} is the surface temperature used for calculating low temperature enthalpy (h_{SO}) using the GASPROPS code,²⁴ and t and t_{REF} are the image time and initial reference time, respectively. Once the temperature maps are converted to heating coefficients, the augmentation effect from the RCS jets can then be directly calculated by comparing the heating with a jet firing to the same condition without the jet firing.

The jet pressure ratio, $P_j/P_{T,2}$, is defined as the ratio of the pressure of the RCS nozzle to the pressure at the stagnation point on the model. This provides a non-dimensional method to compare the RCS performance at different Reynolds numbers and jet blowing pressures. This was also the method used previously to determine jet effectiveness;²⁵ thus providing a way to compare current results with historical results.

III. Results and Discussion

A. PSP Results

The initial focus of this work was to assess the viability of using PSP to measure the pressure changes on the aft-body surface of a capsule reentry vehicle due to the firing of an RCS jet. Towards this goal, all PSP work was performed on an Apollo-era design, due to its simplicity as well as the existence of heating data taken previously on these types of configurations. The Apollo design was also the only aft-body to be coated with copper.

PSP results from the yaw RCS jet at several Reynolds numbers and jet blowing pressures are shown in Fig. 3. The effects on the surface are clearly visible in all of the cases, with the greatest effects occurring at the highest Reynolds number and blowing pressures, which corresponds to the higher $P_j/P_{T,2}$ values. The pressure scale was expanded to negative values to facilitate viewing of the jet effects on the surface. This is more evident when a slice of pressure data is taken near the yaw jet as depicted in Fig. 4. These data show that there is a definite increase in surface pressure due to increasing the jet pressure, but this effect is very small. However, as seen in Fig. 3, it is also apparent that the surface effect from the yaw jet is highly dependent the jet pressure ratio. Visual inspection shows that when the jet pressure is low ($P_j = 1725$ kPa), “augmentation” (or jet effect relative to no jet blowing) seems greatest (though only slightly) at the lowest Reynolds number ($Re = 2.6 \times 10^6/m$), but as the jet pressure is increased, the greatest augmentation is seen at the higher Reynolds number. Finally, it also illustrates that these measurements suffer from a large amount of noise as this is nearing the practical limits of PSP technology. This could possibly be extended by taking significantly more data; however, this was precluded in this facility due to excessive heating that would be experienced with increased run time.

From previous thermal measurements on RCS jet interactions for this model shape,²⁵ a greater pressure response should be seen when the roll RCS jet is employed. This result was confirmed as shown in Fig. 5. Furthermore, visual inspection of the images shows that the greatest augmentation effect is seen at the largest Reynolds number and highest jet blowing pressure. In fact, as the jet pressure ratio is lowered, the augmentation effect actually increases. These results qualitatively agree with results derived from Jones and Hunt using phase-change paints. Representative pressure slices through the jet region (similar to Fig. 4) are shown in Fig. 6 and confirm the higher pressure response including greater signal-to-noise compared with the yaw jet.

B. TSP Results

TSP was used to visualize and quantify the heating effects of the RCS jet interaction to assess its capability for use in hypersonic test facilities. In this experiment, the overall temperature changes on the aft-body should be significantly lower than on the heat shield and approaching the lower limit of the existing thermographic phosphor technique currently used. The temperature changes observed on the aft-body of the model are well within the operating range of the TSP used and exhibit better sensitivity than the existing thermographic phosphor coatings. All TSP measurements were performed on aft-body shapes that were not coated with copper as the nanocomposite material is a good insulator, constraining most if not all of the temperature changes to the surface. A thin, long crack occurred in the TSP coated aft-body during installation of the yaw jet (seen on the lower portion of the model at the yaw jet conditions and labeled in Fig. 7), but all jet interactions occur away from this defect, so its effects were ignored. In addition, the steel fore-body was previously painted with PSP, and since the emission of the PSP is in a different part of the visible spectrum than the TSP (650 nm for the PSP compared to 600 nm for the TSP), the spectral filtering on the camera precluded any visualization of this piece.

To determine if TSP is a viable technique, data from one of the test conditions were compared to ensure that the calculated heating results did not vary appreciably during a given run. This has been shown to be the case using the thermographic phosphor coatings and should hold for TSP as well. Figure 7 depicts several heating images calculated at various times during a run. Visually, all of the images show essentially the same results, and this is further demonstrated if a cut of the heating data is compared for all of the images of the run, as shown in Fig. 8. Disregarding the noise at the beginning of the run (where temperature changes are quite small), the calculated heating values are the same.

Heating results obtained from the RCS yaw jet interaction on the Apollo aft-body are shown in Fig. 9. As opposed to the PSP data above, the interactions are quite clear and show some interesting phenomena. There is also a shock interaction at the jet that is most prevalent at the higher $P_j/P_{T,2}$ values. To quantify the effects of the jet on the surface, a heating augmentation term is defined as the ratio of the heating calculated with the jet on to the heating calculated with the jet off. Using this definition, Fig. 10 shows the heating augmentation effects for the conditions depicted in Fig. 9. This shows that the heating augmentation tends to “broaden” as the $P_j/P_{T,2}$ value increases, but the overall heating augmentation factor is relatively constant. This is also evident when slices of the heating augmentation factors are taken near the jet, as shown in Fig. 11. These data show that the overall heating augmentation for the yaw jet is about 5-6. Physically, this means the capsule experiences an increase in heating by a factor of 5 to 6 in regions where the jet interacts with the surface compared to heating rates when the jet is not being fired. The “broadening” effect of the jet as $P_j/P_{T,2}$ can be seen as the peak heating augmentation is seen farther from the jet at lower $P_j/P_{T,2}$ (Fig. 11a), which moves back towards the jet as the ratio is increased (Fig. 11b).

Heating results from the RCS roll jet interaction are shown in Fig. 12. In this case, the only active roll jet model piece was already coated with PSP, and thus not visible. However, it is probably safe to assume that the immense cooling caused by the expansion of the jet would have been prevalent on the jet piece as well, overshadowing any heating caused by jet interaction on the surface. Similar to the PSP results, in this case, the greatest effect is seen when the $P_j/P_{T,2}$ is relatively large ($> \sim 200$). However, not enough data was collected to determine the actual value where the larger heating effect is seen. Furthermore, at the higher Reynolds number, the jet interaction at the surface actually decreases as the jet blowing pressure increases. This is easily visible when comparing augmentation effects, as in Fig. 13. These data show that the roll jet has a much greater effect on the surface than the yaw jet at all conditions, with maximum augmentation effect being greater than 10 at larger $P_j/P_{T,2}$, and approximately 6 when the $P_j/P_{T,2}$ value is less than 200 (as shown in Fig. 14).

Finally, TSP was applied to an aft-body configuration based on a preliminary design for the Orion vehicle. This design incorporated banks of roll and yaw jets (4 of each) that were to be individually addressable. However, due to testing constraints, only one a configuration in which one of the yaw jets would fire was investigated. The heating results are shown in Fig. 15, and show that contrary to the Apollo configuration, the yaw jet shows little interaction with the surface in both heating intensity as well as spatially. This is most likely due to the slightly different configuration of the jets (for this model, the jets blew outward more than the Apollo configuration). This decrease

in intensity causes a significant decrease in the augmentation effect of the jet, as shown in Fig. 16. The maximum augmentation occurs just aft of the jet exit (as is expected), but quickly decays probably due to the jet wash being entrained into the separation region. The maximum augmentation effect is approximately 2, as shown in Fig. 17, and does not show appreciable dependence $P_j/P_{T,2}$.

IV. Conclusions

The results from a series of proof-of-concept tests to assess the capability of PSP and TSP for hypersonic aerodynamics investigations have been presented. These tests were focused on visualizing and quantifying the interaction of RCS jets on the aft-body of capsule re-entry vehicle shapes (a legacy Apollo era model and a design based on the Orion). Careful experimental system design was needed for the PSP work, taking care to mitigate heating effects on the model surface that would overwhelm the extremely small pressure differences on the model. This was accomplished by coating the Apollo model surface with a thin layer of copper for use as a heat sink. In addition, the lifetime-based method of data acquisition was employed so that all data could be acquired quickly at condition. Using these techniques, the PSP was able to resolve the small pressure gradients on the model. However, existing pressure taps were needed to correct small temperature gradients that biased the data. Using these corrections, the PSP results agreed to within 10% of the measured pressure tap data. From these results, it was shown that the roll jet had much more interaction with the surface than the yaw jet, agreeing qualitatively with heating measurements previously performed on this shape.

TSP experiments were performed on non-copper coated models of both shapes. With the models constructed from an insulating material, most if not all of the heating effects were constrained to the surface. As this was the aft-body of the model, the temperature range measured was ideal for TSP. The temperature gradients were large enough to allow direct comparison of conditions using a “heating augmentation” factor. The TSP results agreed qualitatively with the PSP results and show that this technique could be a viable addition to existing thermographic phosphor coatings to measure aerodynamic heating effects, especially in areas where the temperature range is below the optimum operating range of the phosphor.

Acknowledgements

The authors would like to thank Anthony Robbins for providing support and coordination in the design and fabrication of the high pressure system used for RCS jet simulation, and Kevin Hollingsworth, who, as principle facility engineer, was in charge of conducting the test and ensuring data quality.

References

- ¹Buck, G.M., Watkins, A.N., Danehy, P.M., Inman, J.A., Alderfer, D.W., and Dyakonov, A.A., “Experimental Measurement of RCS Jet Interaction Effects on a Capsule Entry Vehicle,” *46th Aerospace Sciences Meeting*, AIAA, Reno, NV, 2008, Paper 2008-1229.
- ²Kavandi, J., *et al.*, “Luminescence Barometry in Wind Tunnels,” *Rev. Sci. Instrum.*, Vol. 61, No. 11, 1990, pp. 3340-3347.
- ³Morris, M.J., Benne, M.E., Crites, R.C., and Donovan, J.F., “Aerodynamic Measurements Based on Photoluminescence,” *31st Aerospace Sciences Meeting*, AIAA, Reno, NV, 1993, Paper 93-0175.
- ⁴McLachlan, B., and Bell, J., “Pressure-Sensitive Paint in Aerodynamic Testing,” *Exp. Therm. Fluid Sci.*, Vol. 10, No. 4, 1995, pp. 470-485.
- ⁵Liu, T., Campbell, B., Burns, S., and Sullivan, J., “Temperature- and Pressure-Sensitive Luminescent Paints in Aerodynamics,” *Appl. Mech. Rev.*, Vol. 50, No. 4, 1997, pp. 227-246.
- ⁶Liu, T., and Sullivan, J., *Pressure and Temperature Sensitive Paints (Experimental Fluid Dynamics)*, Springer-Verlag, Berlin, 2004.
- ⁷Lakowicz, J., *Principles of Fluorescence Spectroscopy*, 2nd ed., Kluwer Academic/Plenum Publishers, New York, 1999, pp. 239-242.
- ⁸Engler, R., and Klein, C., “DLR PSP System: Intensity and Lifetime Measurements,” *17th International Congress on Instrumentation in Aerospace Simulation Facilities*, IEEE, Pacific Grove, CA, 1997, pp. 46-56.
- ⁹Holmes, J., “Analysis of Radiometric, Lifetime, and Fluorescent Imaging for Pressure Sensitive Paint,” *Aeronaut. J.*, Vol. 102, No. 1014, 1998, pp. 189-194.
- ¹⁰Bell, J.H., Schairer, T.E., Hand, L.A., and Mehta, R.D., “Surface Pressure Measurements Using Luminescent Coatings,” *Annu. Rev. Fluid Mech.*, Vol. 33, 2001, pp. 115-206.
- ¹¹Mitsuo, K., Egami, Y., Asai, K., Suzuki, H., and Mizushima, H., “Development of Lifetime Imaging System for Pressure-Sensitive Paint,” *22nd AIAA Aerodynamic Measurement Technology and Ground Testing Conference*, AIAA, St. Louis, MO, 2002, Paper 2002-2909.

- ¹²Watkins, A.N., Jordan, J.D., Leighty, B.D., Ingram, J.L., and Oglesby, D.M., "Development of Next Generation Lifetime PSP Imaging Systems," *20th International Congress on Instrumentation in Aerospace Simulation Facilities*, IEEE, Gottingen, Germany, 2003, pp. 372-382.
- ¹³Buck, G.M., "An Imaging System for Quantitative Surface Temperature Mapping Using Two-Color Thermographic Phosphors," *34th International Instrumentation Symposium*, ISA, Albuquerque, NM, 1988, pp. 655-663.
- ¹⁴Buck, G.M., "Surface Temperature/Heat Transfer Measurement Using a Quantitative Phosphor Thermography System," *29th Aerospace Sciences Meeting*, AIAA, Reno, NV, 1991, Paper AIAA-91-0064.
- ¹⁵Merski, N.R., "Global Aeroheating Wind-Tunnel Measurements Using Improved Two-Color Phosphor Thermography Method," *J. Spacecraft and Rockets*, Vol. 36, No. 2, 1999, pp. 160-170.
- ¹⁶Daryabeigi, K., "Global Surface Temperature/Heat Transfer Measurements Using Infrared Imaging," *17th Aerospace Ground Testing Conference*, AIAA, Nashville, TN, 1992, Paper 92-3959.
- ¹⁷Gallery, J., Gouterman, M., Callis, J., Khalil, G., McLachlan, B., and Bell, J., "Luminescent Thermometry for Aerodynamic Measurements," *Rev. Sci. Instrum.*, Vol. 65, No. 3, 1994, pp. 712-720.
- ¹⁸Fey, U., Engler, R.H., Egami, Y., Iijima, Y., Asai, K., Jansen, U., and Quest, J., "Transition Detection Using temperature Sensitive Paint at Cryogenic Temperatures in The European Transonic Wind Tunnel (ETW)," *20th International Congress on Instrumentation in Aerospace Simulation Facilities*, IEEE, Gottingen, Germany, 2003, pp. 77-88.
- ¹⁹Hamner, M. P., Popernack, T. G., Jr., Owens, L. R., and Wahls, R. A., "Using Temperature Sensitive Paint Technology," *40th Aerospace Sciences Meeting*, AIAA, Reno, NV, 2002, Paper 2002-0742.
- ²⁰Oglesby, D.M., and Upchurch, B.T., "In Pursuit of the Ideal Pressure Sensitive Paint," *7th Annual Pressure Sensitive Paint Workshop*, Purdue University, West Lafayette, IN, 1999.
- ²¹Micol, J.R., "Langley Aerothermodynamic Facilities Complex: Enhancements and Testing Capabilities," *36th Aerospace Sciences Meeting*, AIAA, Reno, NV, 1998, Paper 1998-0147.
- ²²Carslaw, H.S., and Jaeger, J.C., *Conduction of Heat in Solids*, 2nd ed., Oxford University Press, London, 1959.
- ²³Fay, J.A., and Riddell, F.R., "Theory of Stagnation Point Heat Transfer in Dissociated Air," *J. Aero. Sci.*, Vol. 25, 1958, pp. 73-85.
- ²⁴Hollis, B.R., "Real-Gas Flow Properties for NASA Langley Research Center Aerothermodynamics Facilities Complex Wind Tunnels," NASA CR 4755, September 1996.
- ²⁵Jones, R.A., and Hunt, J.L., "Effects of Cavities, Protuberances, and Reaction-Control Jets on Heat Transfer to the Apollo Command Module," NASA TM X-1063, March 1965.

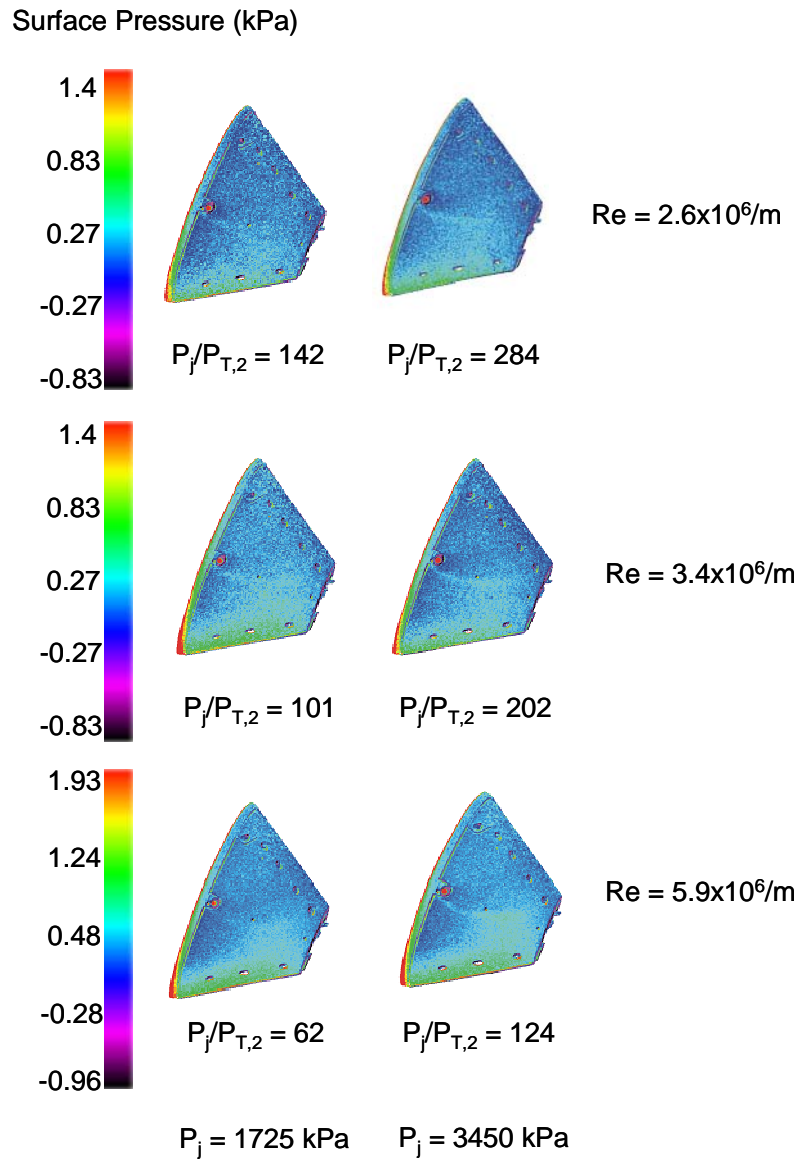


Figure 3. PSP results from the Apollo configuration at increasing Reynolds number (Re) and different RCS yaw jet blowing pressure (P_j).

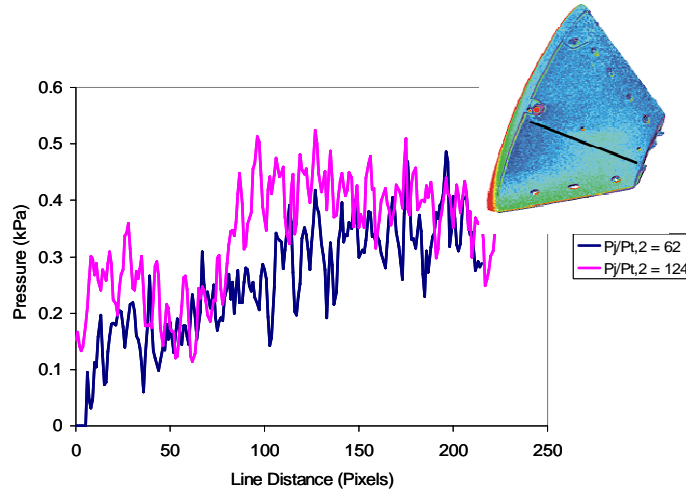


Figure 4. Line cut of PSP data recovered for the Apollo configuration at $Re = 5.9 \times 10^6/m$ at different yaw jet blowing pressures. The line in the inset shows the approximate location of the cut.

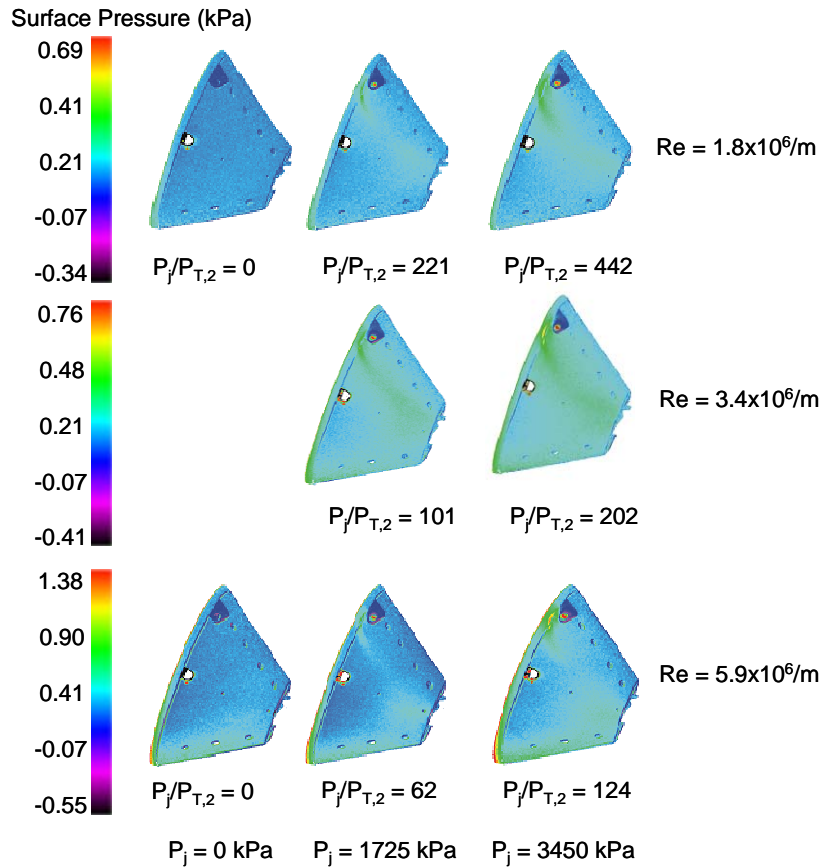


Figure 5. PSP results from the Apollo configuration at increasing Reynolds number and different RCS roll jet blowing pressure.

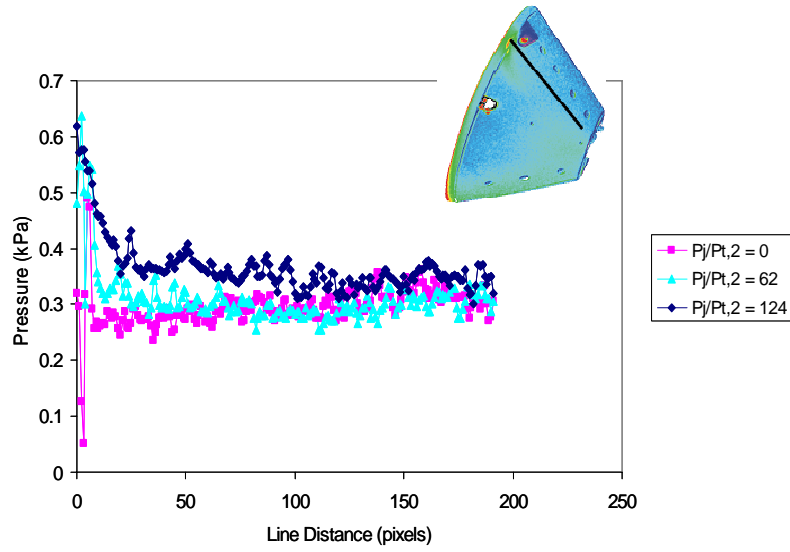


Figure 6. Line cut of PSP data recovered for the Apollo configuration at $Re = 5.9 \times 10^6/m$ at different roll jet blowing pressures. The line in the inset shows the approximate location of the cut.

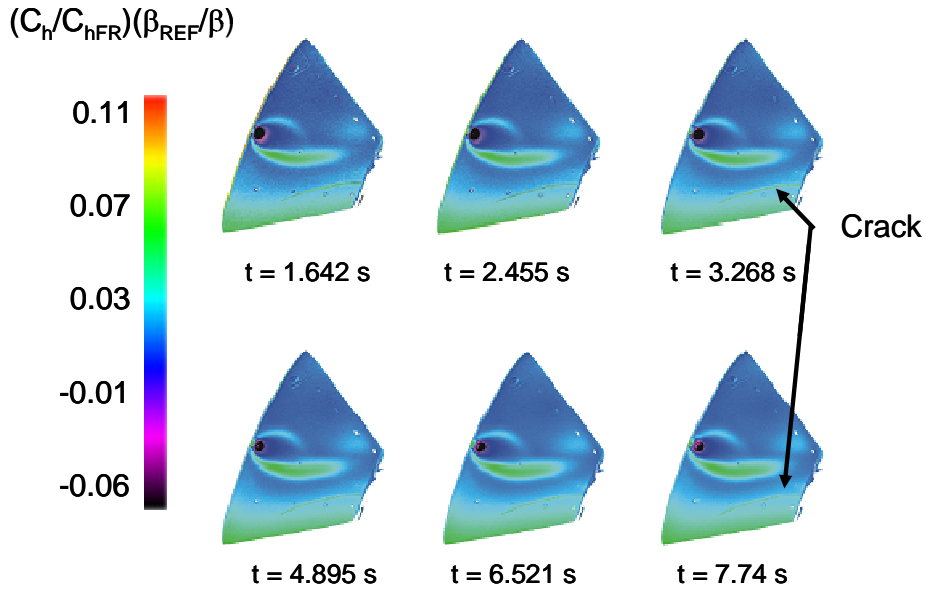


Figure 7. Representative heating images recovered using TSP on the Apollo configuration at $Re = 0.56 \times 10^6$ and yaw jet blowing pressure of 3450 kPa. The location of the thin crack is also depicted.

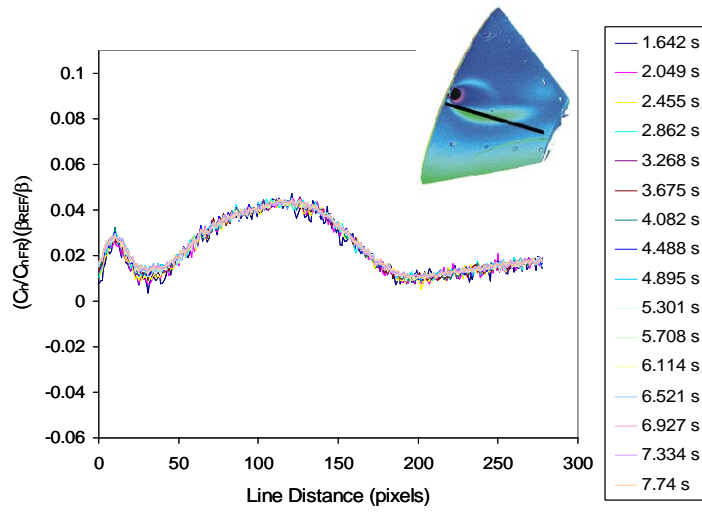


Figure 8. Heating data calculates throughout an entire run. Tunnel conditions are the same as in Fig. 7. The inset shows the approximate location of the slice.

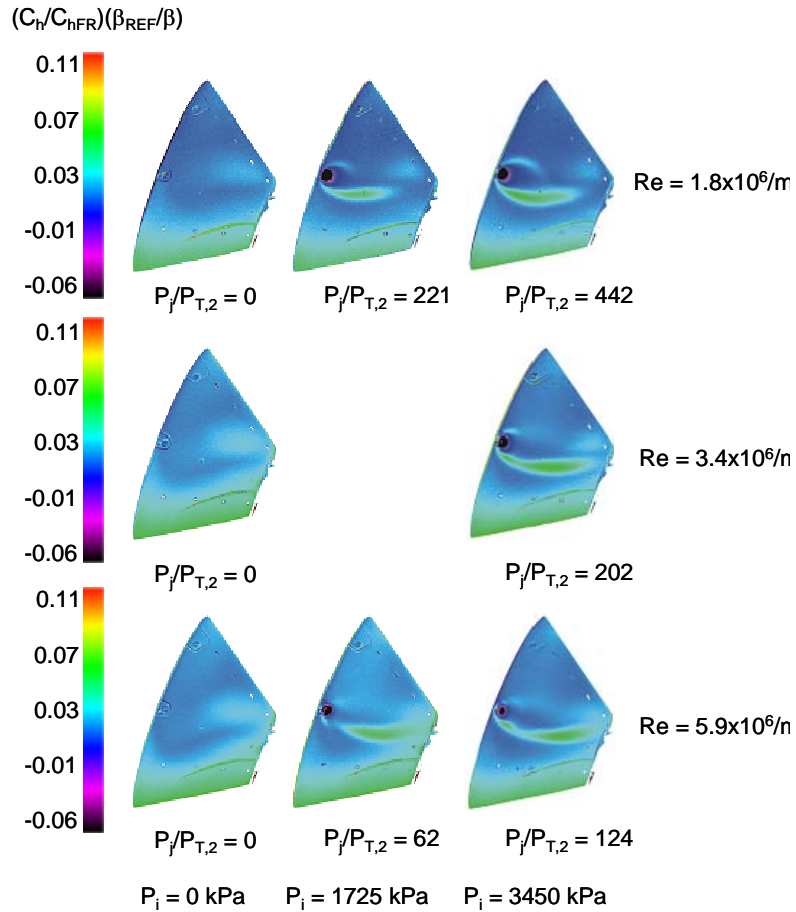


Figure 9. Heating images recovered using TSP for the Apollo configuration at various Reynolds numbers and yaw jet blowing pressures.

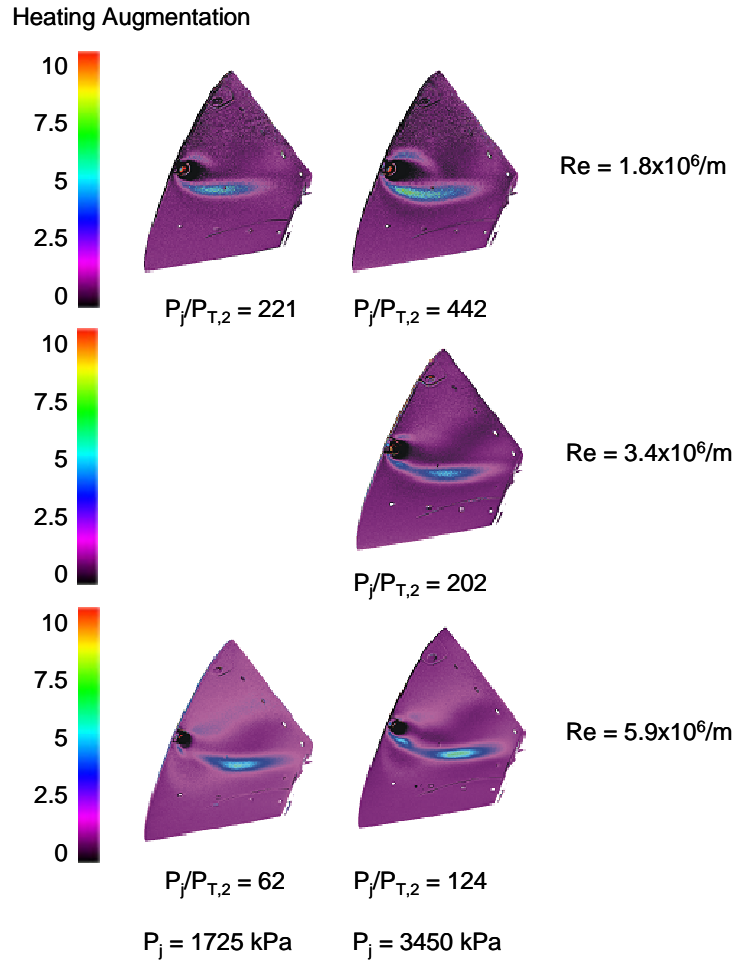


Figure 10. Heating Augmentation factors calculated for yaw jet firing on the Apollo configuration.

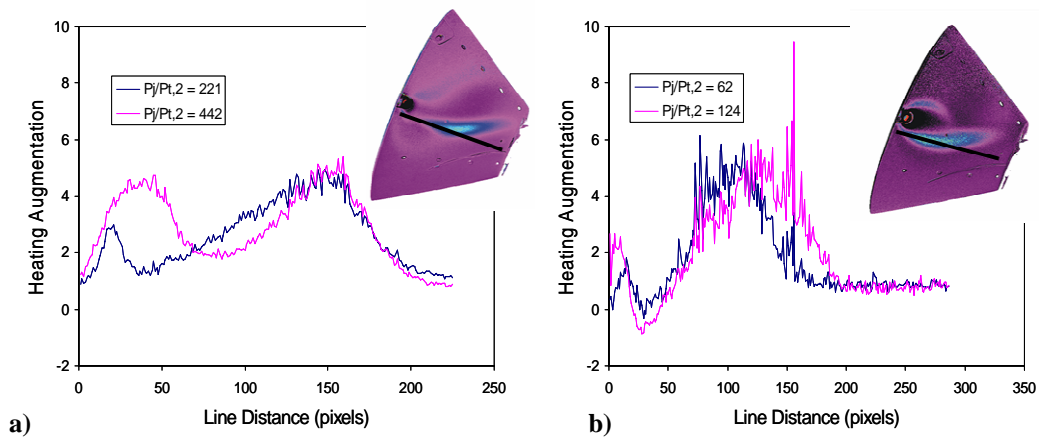


Figure 11. Slices of the augmentation factors showing the effect of the yaw RCS jet. The insets show the approximate location of the slice. a) $\text{Re} = 5.9 \times 10^6/\text{m}$; b) $\text{Re} = 1.8 \times 10^6/\text{m}$

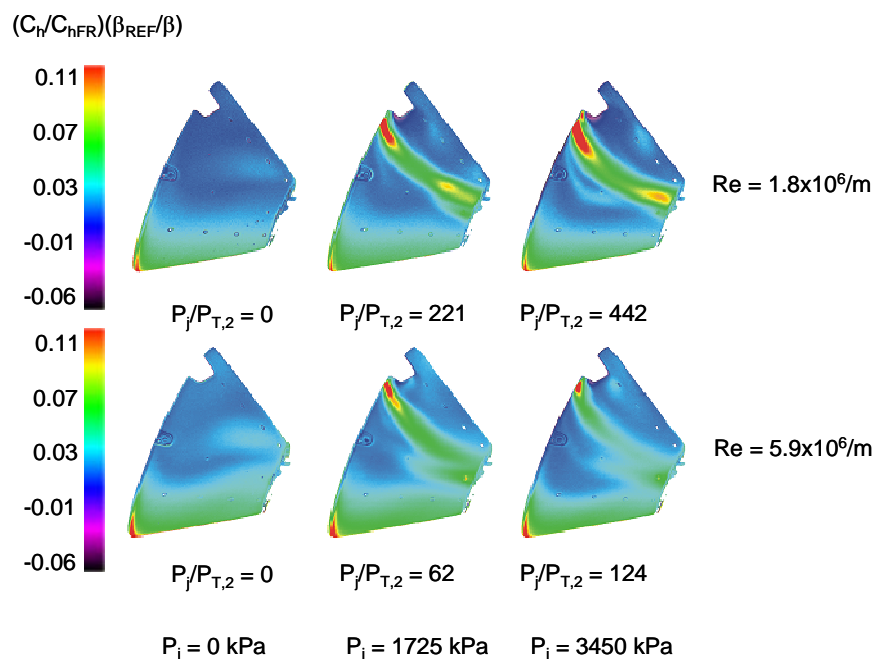


Figure 12. Heating images recovered using TSP for the Apollo configuration at various Reynolds numbers and roll jet blowing pressures.

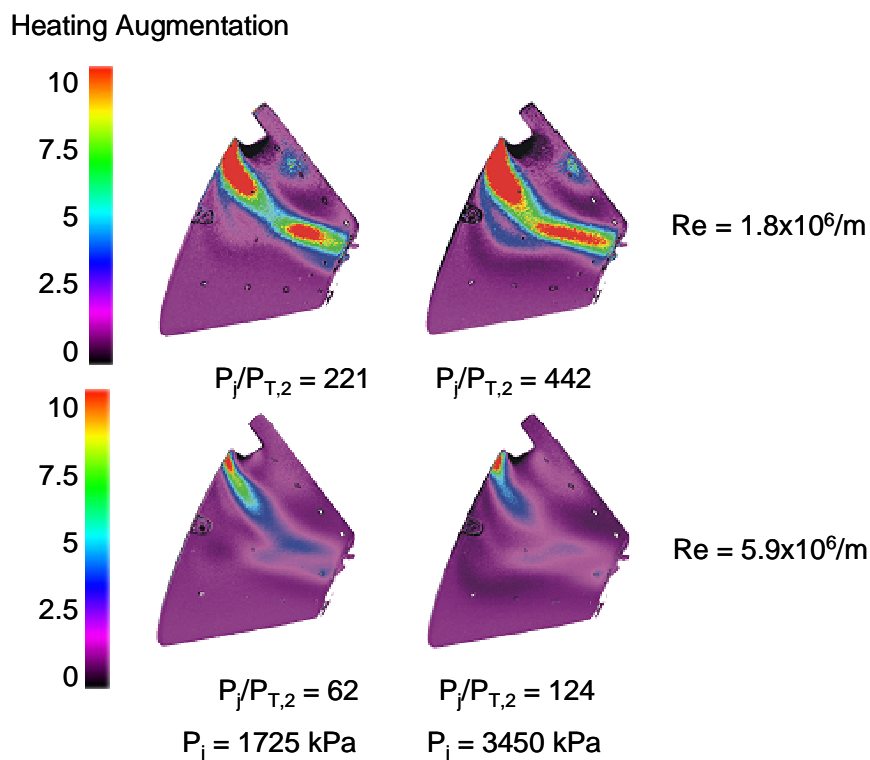


Figure 13. Augmentation factors calculated for roll jet firing on the Apollo configuration.

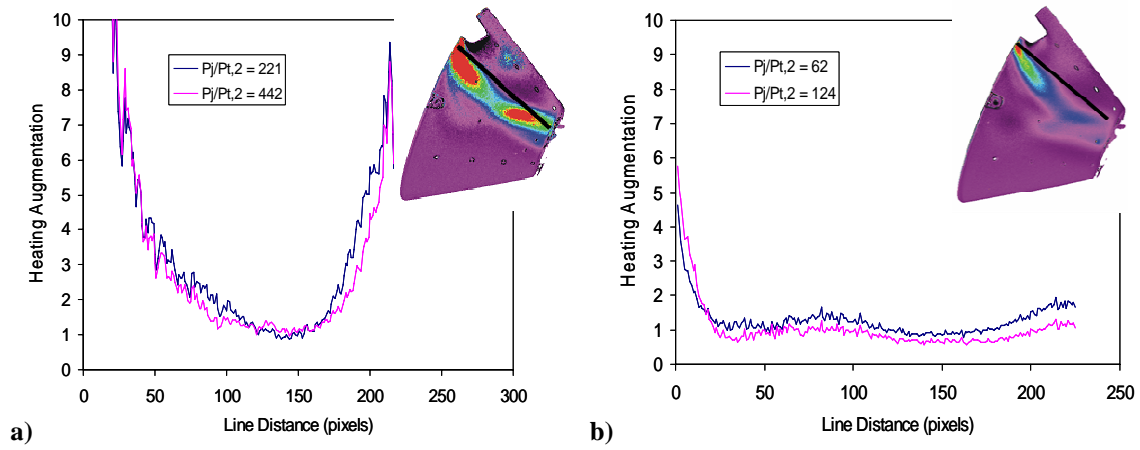


Figure 14. Slices of the augmentation factors showing the effect of the roll RCS jet. The insets show the approximate location of the slice. a) $Re = 1.8 \times 10^6/m$; b) $Re = 5.9 \times 10^6/m$

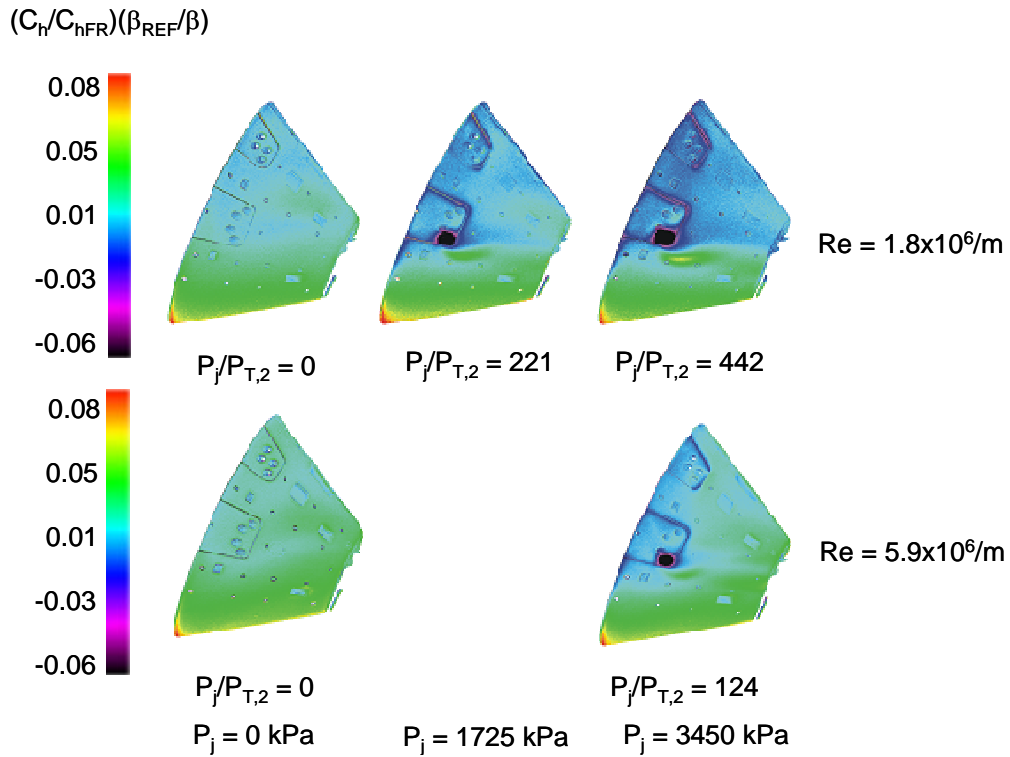


Figure 15. Heating images recovered using TSP for the Orion configuration at various Reynolds numbers and yaw jet blowing pressures.

Heating Augmentation

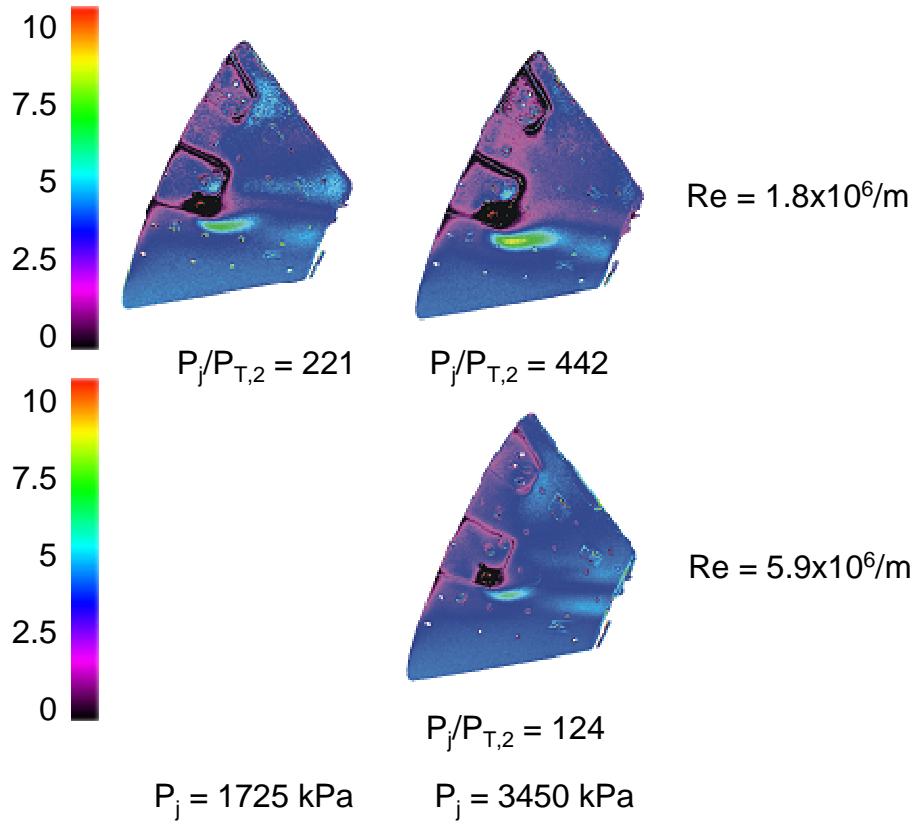


Figure 16. Augmentation factors calculated for yaw jet firing on the Orion configuration.

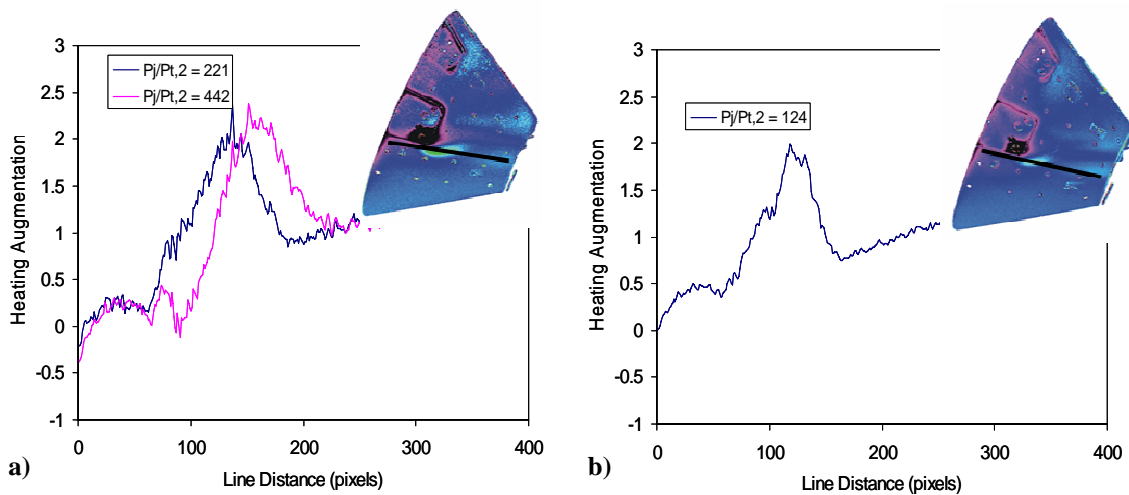


Figure 17. Slices of the augmentation factors showing the effect of the yaw RCS jet. The insets show the approximate location of the slice. a) $\text{Re} = 1.8 \times 10^6/\text{m}$; b) $\text{Re} = 5.9 \times 10^6/\text{m}$